This is an *Accepted Manuscript*, which has been through the Royal Society of Chemistry peer review process and has been accepted for publication.

Accepted Manuscripts are published online shortly after acceptance, before technical editing, formatting and proof reading. Using this free service, authors can make their results available to the community, in citable form, before we publish the edited article. We will replace this *Accepted Manuscript* with the edited and formatted *Advance Article* as soon as it is available.

You can find more information about *Accepted Manuscripts* in the **Information for Authors**.

Please note that technical editing may introduce minor changes to the text and/or graphics, which may alter content. The journal's standard **Terms & Conditions** and the **Ethical guidelines** still apply. In no event shall the Royal Society of Chemistry be held responsible for any errors or omissions in this *Accepted Manuscript* or any consequences arising from the use of any information it contains.

Journal Name

ARTICLE

Solvent-induced construction of two zinc metal-organic frameworks with high selective detection for nitroaromatic explosives

Chuanqi Zhang, Yan Yan, Libo Sun, Zhiqiang Liang* and Jiyang Li*

Two novel zinc metal-organic frameworks $[Zn_3(TPT)_2(DMF)_2]\cdot0.5HNMe_2$ (**1**) and $NH_2Me_2\cdot[Zn(TPT)]\cdot DMF$ (**2**) have been synthesized by using Zn (II) ions and p-terphenyl-3,4'',5 tricarboxylate acid (H_3TPT). The structures of these two MOFs are dependent on the solvents used in the synthetic processes. Compound **1** was synthesized in a mixture of DMF and H_2O, while compound **2** was obtained in the presence of DMF and ethanol. The three-dimensional (3D) framework of **1** is constructed by the connection of Zn-carboxylate chains and TPT^{3-} linkers. Structure of **2** can be described as a 3,6-connected network based on the assembly of bi-nuclear zinc clusters and TPT^{3-} ligands. These two MOFs exhibit ligand-based photoluminescence at around 375 nm, as well as high efficiency for the recyclable detection of nitroaromatic explosives.

Introduction

Nowadays, metal-organic frameworks (MOFs), as a new kind of functional materials, have attracted tremendous interests because of their potential applications in adsorption,[1-4] molecular recognition,[5-7] catalysis,[8-10] optics[11, 12] and magnetism.[13, 14] The complicated structures of MOFs constructed by the assembly of metal ions (or clusters) and organic ligands are quite difficult to predict and control in the synthesis. Some physical or chemical factors, such as temperature, counterion, pH value, metal-to-ligand ratio, solvent, etc., have unpredictable impacts on the structures and properties of the resulting MOFs.[15-20] Among these factors, solvent effects have been well demonstrated previously, which can control the pore size and interpenetration of MOFs,[21-23] resulting in the structural diversities and structurally-related properties.[24-27] For example, Su et al. have successfully synthesized a series of porous Zn-BTC (BTC = 1,3,5-benzenetricarboxylate) MOFs with different structures and pore sizes by using varisized solvents.[21]

The massive misuse of nitroaromatic compounds (NACs) throughout the world have not only brought terrible terror attacks, but also caused serious pollution to the environment. Therefore, highly sensitive detection of NACs has become a critical issue. Luminescent metal-organic frameworks (LMOFs) with tunable permanent porosity and electronic structure may pre-concentrate and recognize the targeted analytes, leading to high sensitivity and selectivity.[28-30] These unique features make LMOFs as promising candidates for detecting NACs.[31, 32] For examples, a luminescent microporous $Zn_2(bpdc)_2(bpee)$ was used for the fast and reversible detection of 2,4-dinitrotoluene and 2,3-dimethyl-2,3-dinitrobutane in the vapor phase.[33] Du et al. utilized a microporous metal-organic anionic framework $[In_2L][NH_2(CH_3)_2]_2\cdot(DMF)_4(H_2O)_{16}$ (L = tetrakis[(3,5-dicarboxy-phenoxy)methyl] methane) for the highly sensitive detection of nitrobenzene in both vapor and liquid phases.[34]

In this work, we selected the rigid low symmetrical tricarboxylate ligand *p*-terphenyl-3,4'',5-tricarboxylic acid (H_3TPT)[35,36] to construct two LMOFs ($[Zn_3(TPT)_2(DMF)_2]\cdot0.5HNMe_2$ (**1**) and $NH_2Me_2\cdot[Zn(TPT)]\cdot DMF$ (**2**) by controlling the solvents, and further studied their sensing abilities for the detection of NACs. **1** possesses the infinite metal-carboxylate chains, which are further linked into a 3D framework by TPT^{3-} ligands. In the structure of **2**, adjacent Zn^{2+} ions are bridged by six TPT^{3-} linkers to form binuclear $[Zn_2(COO)_6]$ building units, which are further connected by the TPT^{3-} ligands to generate an anionic 3D framework. Both of them show ligand-based photoluminescence at room temperature, and their micrometer-sized samples (**1'** and **2'**) can be used as chemical sensors for the detection of NACs.

Experimental section

Materials and methods

H_3TPT was prepared according to our previous work.[35, 36] All metal salts, solvents and organic reagents were of reagent grade quality and used without further purification. The IR absorption

spectra were recorded in the range of 400–4000 cm^{-1} on a Nicolet 6700 FT-IR spectrometer with KBr pellets. Powder X-ray diffraction (PXRD) patterns were collected on a Rigaku D-Max 2550 diffractometer using Cu-Kα radiation (λ = 0.15418 nm) in a 2θ range of 4–40° at room temperature. The element analyses were performed using a Perkin-Elmer 2400 elemental analyzer. Thermogravimetric analyses (TGA) were performed on Perkin-Elmer TGA-7 thermogravimetric analyzer from room temperature to 800 °C in air atmosphere with a heating rate of 10 $^{\circ}$C/min. The fluorescence spectra were recorded on a SHIMADZU RF-5301 PC fluorescence spectrophotometer. The point symbol and topological analyses were conducted by using TOPOS program package.[37, 38]

Crystal structure determination

Single-crystal X-ray diffraction data for **1** and **2** were recorded by using a Bruker AXS SMART APEX-□ diffractometer with graphite monochromated Mo Kα (λ = 0.71073 Å) radiation at 293 K. Data processing was completed with the SAINT processing program.[39] The structures of **1** and **2** were solved by the direct method and refined on F^2 by full-matrix least-squares with the SHELX-97 program.[40] All non-hydrogen atoms were refined with anisotropic displacement parameters. Hydrogen atoms on the aromatic rings were placed geometrically with isotropic thermal parameters 1.2 times of that of the attached carbon atoms. A summary of the crystallographic data and refinement parameters are given in Table S1. The selected bond lengths and angles of **1** and **2** are given in Table S2 and Table S3, respectively.

Synthesis of [Zn$_3$(TPT)$_2$(DMF)$_2$]·0.5HNMe$_2$ (1)

Zn(OAc)$_2$·2H$_2$O (5.50 mg, 0.025 mmol), H$_3$TPT (2.28 mg, 0.0063 mmol) and morpholine (1.72 mg, 0.02 mmol) were dissolved in a mixture of DMF (1.8 mL) and H$_2$O (0.2 mL), and then HNO$_3$ (60 uL, 2 M) was added. The mixed solution was sealed in a 20 mL vial and heated at 85 $^{\circ}$C for 48 hours, then cooled to room temperature. Colourless block-shaped crystals of **1** were collected by filtration, washed with the mother liquid and dried at room temperature (45% yield). Anal. Calcd for C$_{49}$H$_{39.5}$N$_{2.5}$O$_{14}$Zn$_3$: C 54.31, H 3.67, N 3.23. Found: C 53.81, H 3.89, N 3.94. IR (KBr, cm^{-1}): 3157(w), 3034(w), 2926(w), 2789(w), 1640(s), 1584(m), 1460(m), 1427(m), 1360(s), 1245(w), 1088(m), 1010(m), 930(w), 835(m), 775(s), 728(m), 635(m), 557(w), 493(w).

Synthesis of NH$_2$Me$_2$·[Zn(TPT)]·DMF (2)

Compound **2** was obtained under the similar reactions but using 2 mL solution of DMF-ethanol (9:1, v/v) as the solvent instead of 2 mL DMF-H$_2$O (9:1, v/v). Colourless plate crystals of **2** were collected by filtration, washed with the mother liquid and dried at room temperature (63% yield). Anal. Calcd for C$_{26}$H$_{26}$N$_2$O$_7$Zn: C 57.41, H 4.82, N 5.15. Found: C 57.90, H 4.80, N 5.12. IR (KBr, cm^{-1}): 3385(w), 3158(w), 3045(w), 2933(w), 1649(s), 1591(m), 1450(w), 1422(m), 1366(s), 1243(w), 1092(m), 10160(w), 836(w), 771(s), 732(m), 657(m), 563(m), 486(w).

Synthesis of the micrometer-sized phase of 1'

Zn(OAc)$_2$·2H$_2$O (220 mg, 1.0 mmol), H$_3$TPT (91.2 mg, 0.25 mmol) and morpholine (68.8 mg, 0.8 mmol) were dissolved in 40 mL of DMF-H$_2$O (9:1, v/v), and then HNO$_3$ (2.4 mL, 2 M) was added. The mixture was sealed in a 100 mL flask and heated at 85 $^{\circ}$C with stirring on an oil bath for 48 hours. When the reaction mixture was cooled to room temperature, the product was collected from the mother liquid by centrifugation and dried under ambient conditions. The PXRD pattern shows that **1'** has the same structure with **1**.

Synthesis of the micrometer-sized phase of 2'

The synthesis of **2'** is similar to that of **1'** except for 40 mL solution of DMF-ethanol (9:1, v/v) used as the solvent. The PXRD pattern also indicates that the **2'** has the same structure with **2**.

Detection experiments for solvents and nitroaromatic compounds

The micrometer-sized samples **1'** and **2'** were used for the detection experiments by taking advantage of their excellent dispersible nature, which might facilitate the close contact between the host frameworks and analytes. The solvent sensing experiments were carried out as following: the micrometer-sized samples of **1'** and **2'** (2 mg) were well dispersed in different solvents (2 mL) by stirring for 30 minutes to prepare stable suspensions, and then the fluorescence of these suspensions was recorded, respectively. For the detection experiments of NACs, 0.5 mg of **1'** and **2'** were uniformly dispersed in 2 mL ethanol, fluorescence quenching was monitored by photoluminescence (PL) spectroscopy when the NACs were added to ethanol suspensions.
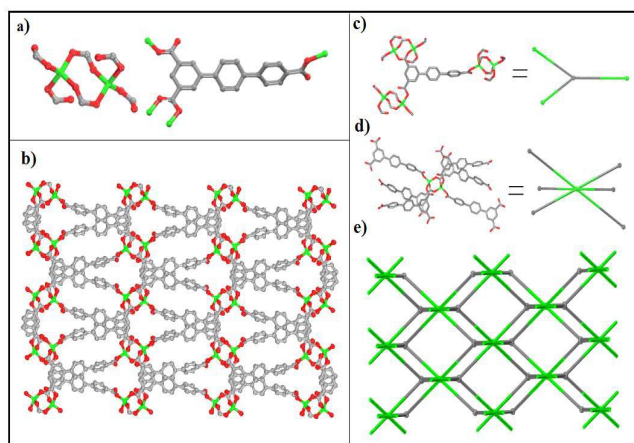
Result and discussion

Crystal structure

Single crystal X-ray structural analyses reveal that **1** crystallizes in monoclinic *C*2/*c* space group. The asymmetric unit contains one and a half Zn(II) ions, one TPT^{3-} ligand, one coordinated DMF molecule, and one half of dimethylamine guest molecule formed by the decomposition of DMF molecules (Fig. S1a). There are two types of coordination modes for Zn atoms: one exhibits a distorted tetrahedral geometry, which is four-coordinated by four oxygen atoms from TPT^{3-} linkers; the other one is octahedrally coordinated by four oxygen atoms belonging to four TPT^{3-} linkers and two oxygen atoms from coordinated DMF molecules (Fig. 1a). In the structure of **1**, the three carboxylate groups of TPT^{3-} ligands adopt the bridging bismonodentate mode to coordinate with six zinc atoms (Fig. 1b). As shown in Fig. 1c–d, three Zn centers are linked by carboxylate groups to generate a metallic trimer Zn$_3$(CO$_2$)$_6$ subunit, which is further assembled by carboxylate groups to form an infinite metal-carboxylate chain. These metal-carboxylate chains are connected by isophthalic moieties to generate 2D networks, which are further linked by TPT^{3-} ligands to construct a 3D framework. **1** shows a 4,8-connected binodal net with an *alb*-4,8-*C*2/*c* topology with point symbol of $(4^4·6^2)_2(4^8·6^{17}·8^3)$ upon considering the metallic trinuclear Zn$_3$(CO$_2$)$_6$ as a 8-connected node and the TPT^{3-} ligand as a 4-connected linker (Fig. 1e–g).
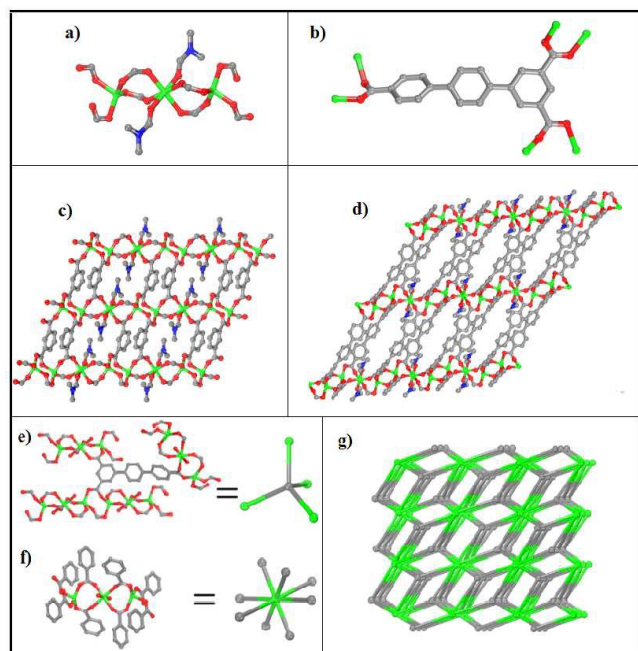
Fig. 1 a) Metallic trimer $Zn_3(CO_2)_6$ subunit; b) Coordination modes of carboxyl groups of TPT^{3-} ligand; c) View of 2D layer constructed by metal-carboxylate chains and isophthalic moieties; d) View of 3D framework formed by metal-carboxylate chains and TPT^{3-} ligands; e), f) Ball-and-stick representations of 4-connected and 8-connected nodes, respectively (the coordinated DMF molecules are omitted for clarity); g) Schematic representation of 4,8-connected alb-4,8-$C2/c$ topology of **1** (color modes: Zn green, O red, C gray).

Fig. 2 a) Dimeric $[Zn_2(COO)_6]$ subunit and coordination mode of carboxyl groups of TPT^{3-} ligand in **2**; b) View of 3D framework constructed by the assembly of dimeric $[Zn_2(COO)_6]$ subunits and TPT^{3-} ligands; c), d) Ball-and-stick representations of 3-connected (gray) and 6-connected nodes (green), respectively; e) Schematic representation of 3,6-connected scu-3,6-*Pbcn* topology of **2** (color modes: Zn green, O red, C gray).
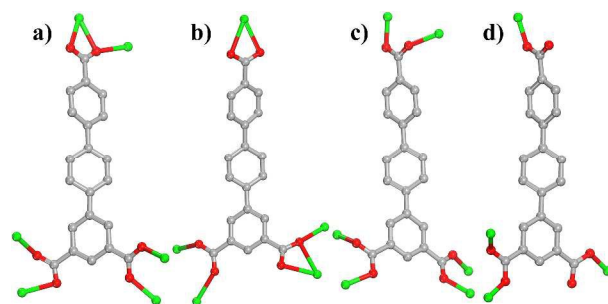
Fig. 3 Summary of diverse coordination modes of H_3TPT in the synthesized MOFs: a) Cd-TPT, b) La-TPT, c) **1**, d) **2** (colour modes: metal, green; oxygen, red, carbon, gray).

When the mixed solvents DMF-H_2O was changed to DMF-ethanol, $NH_2Me_2 \cdot [Zn(TPT)] \cdot DMF$ (**2**) with distinct structure was formed. Compound **2** crystalizes in orthorhombic *Pbcn* space group. The asymmetric unit of **2** contains one Zn(II) atom, one TPT^{3-} ligand, one DMF molecule and one $[(CH_3)_2NH_2]^+$ cation arised from the degradation of DMF molecules (Fig. S1b). As illustrated in Fig. 2a−b, different from the two types of zinc atoms in **1**, zinc atoms in **2** are tetrahedrally coordinated to four oxygen atoms from four different TPT^{3-} ligands. Two Zn atoms are bridged by six TPT^{3-} ligands to form a dimeric but non-paddle-wheel $[Zn_2(COO)_6]$ subunit. The carboxylate groups of TPT^{3-} ligand in **2** exhibit two different kinds of coordination modes, the monodentate mode and the bridging bismonodentate mode, to connect $[Zn_2(COO)_6]$ subunits to generate a 3D anion framework with 1D rhombic channel along the [001] direction, the pore dimension is ca. 8.5 × 9.4 Å (van der Waals radii of the atoms have been taken in account) (Fig. S2). The negative charge of $[Zn(TPT)]^-$ framework is balanced by dimethylammonium cations residing in the channels. From the topological viewpoint, dimeric $[Zn_2(COO)_6]$ subunits connected by six carboxylate groups can be viewed as 6-connected nodes, and TPT^{3-} ligands act as 3-connected nodes. Thus, **2** can be simplified to a (3,6)-connected scu-3,6-*Pbcn* net with point symbol of $(4.6^2)_2(4^2.6^9.8^3.10)$ (Fig. 2c−e).

From the above discussion, it is clear that the different constituents of solvents result in the different structural arrangements for **1** and **2**. The ethanol and water molecules in the mixed solvents are not incorporated into the structures, while DMF molecules are coordinated to zinc ions as terminal molecules in **1** and incorporated into **2** as guests, respectively. In addition, the different coordination modes of the metal clusters (the $Zn_3(CO_2)_6$ trinuclear subunits for **1** and the $Zn_2(COO)_6$ binuclear subunits for **2**) and carboxylate groups of TPT^{3-} ligands are observed in **1** and **2**, and the structural discrepancies of these two compounds may be supposed to be the result of the coordination competition between carboxylate and individual solvent.[25, 41]

Coordination modes of H_3TPT in the synthesized MOFs

There are two kinds of distinct carboxyl groups on the two different phenyl rings in H_3TPT ligand: benzoic acid and isophthalic acid. These carboxyl groups could display different coordination modes in the syntheses of MOFs. In previous works, we have synthesized cadmium and lanthanum MOFs (Cd-TPT and La-TPT) with luminescent properties using H_3TPT.[35, 36] A summary of the diverse coordination modes of H_3TPT ligand is shown in Fig. 3. The three carboxylate groups of TPT^{3-} linker in Cd-TPT adopt two different coordination modes: the μ_3-chelating-bridging tridentate node and the bridging bismonodentate (Fig. 3a).[35] While in the structure of

La-MOF, three carboxylic groups adopt three distinct coordination modes to link the La ions (Fig. 3b). In compound **1**, the three carboxylate groups of TPT[3-] ligand adopt the bridging bismonodentate mode to coordinate with six zinc atoms (Fig. 3c).[36] The carboxylate groups of TPT[3-] ligand in **2** exhibit the monodentate mode and the bridging bismonodentate mode (Fig. 3d). This shows that H_3TPT ligand can adopt different coordination modes to facilitate the construction of MOFs with diverse topologies.

PXRD, IR and TG analyses

The purities of the as-synthesized **1**, **2** and their micrometer-sized samples have been confirmed by their PXRD patterns (Fig. S3). The PXRD patterns indicate that the structures of **1'** and **2'** match well with that of **1** and **2**, respectively. The SEM images of **1'** and **2'** show plate-like and block-shaped morphologies with a scale of several micrometers, respectively (Fig. S4). The IR spectra are recorded to characterize the functional groups of **1** and **2**. As shown in Fig. S5, the absence of absorption around 1700 cm^{-1} further confirms that the H_3TPT ligands are completely deprotonated. The TGA curve of **1** shows an obvious weight loss of 19.5% from 180 °C to 300 °C, corresponding to the loss of dimethylamine guest molecules and coordinated DMF molecules (calcd. 17.7%). There is a plateau between 300 °C and 450 °C, then the sample starts to decompose with a total weight loss of 78.8% to form ZnO (calcd. 77.4%). For **2**, the first weight loss of 23.4% from 170 °C to 360 °C arises from the loss of dimethylammonium cations and DMF guest molecules (calcd. 21.9%). The sample starts to decompose at 420 °C and ends at 550 °C with a total weight loss of 84.3% to form ZnO (calcd.85.0%).

Luminescent properties and sensing behaviors

Considering that metal-organic frameworks constructed by d^{10} metal ions and conjugated organic ligands are promising candidates for potential photoactive materials,[22] the solid PL spectra of H_3TPT ligand, **1** and **2** were recorded at room temperature. As shown in Fig. 4, **1** and **2** show emissions at 383 nm and 375 nm upon excitation at 330 nm and 334 nm, respectively. Compared with the maximum emission of H_3TPT at 445 nm upon excitation at 370 nm, the obvious blue-shift of **1** and **2** can be assigned to the strong electrostatic interaction between Zn^{2+} and the TPT[3-] ligands.[42, 43] Moreover, the PL quantum yields are 5.66%, 13.27% and 13.37% for H_3TPT ligand, **1** and **2**, respectively.

In view of the excellent dispersible nature of micrometer-sized sample, **1'** and **2'** were used to investigate their luminescence properties in different solvents. The solvents used were methanol, ethanol, acetone, acetonitrile, dimethylsulfoxide (DMSO), tetrahydrofuran (THF), and nitrobenzene (NB). As shown in Fig. 5, the PL spectra of suspensions of **1'** and **2'** in different solvents show ligand-based emissions around 370 nm, which are similar to their solid state emission spectra. It is noteworthy that **1'** and **2'** respond differently to the solvent molecules, NB exhibits the most effect quenching behavior for both **1'** and **2'**.
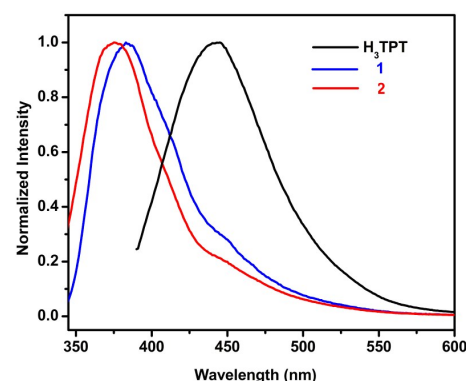

Fig. 4 Emission spectra of H_3TPT, and **1** and **2** in solid state upon excitation at 370 nm, 330 nm and 334 nm.
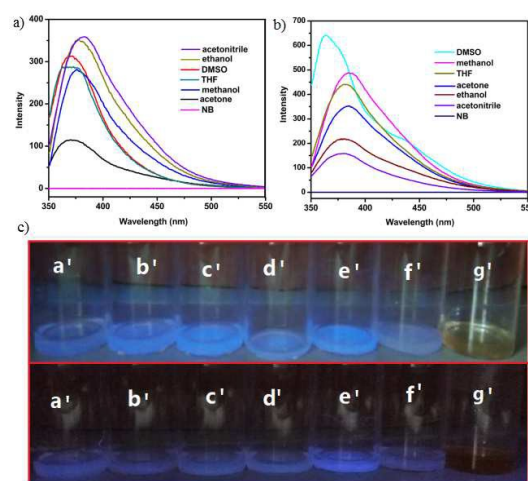

Fig. 5 a), b) Emission spectra of **1'** and **2'** in different solvents when excited at 319 nm and 335 nm, respectively; c) Photographs of **1'** (up) and **2'** (below) under UV light (max = 365 nm) in different solvents (a' = DMSO, b' = ethanol, c' = acetonitrile, d' = THF, e' = methanol, f' = acetone, g' = NB).

Detection for nitroaromatic compounds

The primary results of the quenching behavior of NB motivated us to further examine the sensing abilities of **1'** and **2'** toward other NACs. 2,4,6-Trinitrotoluene (TNT), 2,4-dinitrotoluene (2,4-DNT), 4-nitrotoluene (4-NT), 2-nitrotoluene (2-NT), 4-nitrobenzaldehyde (4-NBA), nitrobenzene (NB), 4-nitrophenol (4-NP), 2,4-dinitrophenol (2,4-DNP) and picric acid (PA) were added to ethanol suspensions of **1'** and **2'** to investigate their corresponding luminescence responses. As shown in Fig. 6a−b, Fig. S7 and Fig. S8, these NACs display a varying degree of fluorescence quenching for the suspensions. Insignificant quenching effects have been observed for NB, 4-NBA, TNT, 2,4-DNT and 4-NT, however, hydroxy-substituted NACs: 4-NP, 2,4-DNP, especially PA can effectively quench the emissions of **1'** and **2'** suspensions. The emission intensities of **1'**, **2'** suspensions decrease to 20% and 11% in presence of only 11 ppm of PA, respectively (Fig. 7). These results indicate that both the two compounds have the potentialities for selective detection of 4-NP, 2,4-DNP and PA over their methyl-substituted analogues. Furthermore, the quenching efficiency of

the NACs can be evaluated based on Stern-Volmer (SV) equation: $I_o/I = 1 + K_{sv} \times [M]$, where I_o and I are the luminescent intensities before and after the addition of respective NACs; [M] is the molar concentration of NACs and K_{sv} is the quenching constant. It is noteworthy that the S-V plots of PA of **1'** and **2'** are almost linear at low concentrations and bend upwards at higher concentrations (Fig. 6c−d). The quenching constants for PA are found to be 6.39×10^4 M^{-1} and 7.18×10^4 M^{-1} for **1'** and **2'**, respectively, which are comparable or higher than that of other literature known MOF-based chemosensors.[44-46] Although there are distinct structural discrepancies in **1** and **2**, they exhibit the similar sensing performances towards NACs because the absence of porosity in their structures, and the quenching process occurs primarily due to the surface adsorption of the NACs on the MOF particles.[47]
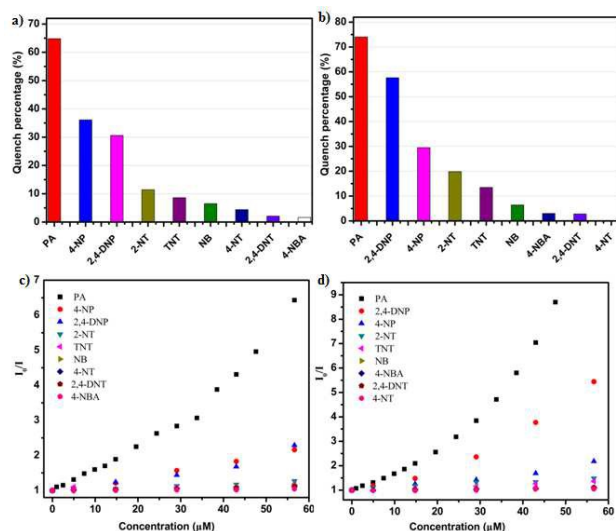

Fig. 6 a), b) Reduction of luminescent intensities (plotted as quench percentage) of **1'** and **2'** in present of different NACs with the concentration of 29.1 μM, respectively; c), d) Stern–Volmer (SV) plots for various NACs in ethanol for **1'** and **2'**, respectively.

The non-linear S-V plots for PA suggests that a resonance energy transfer mechanism occurs in fluorescence quenching.[44, 48] The probability of energy transfer depends on the extent of spectral overlap between the absorption spectra of NACs and the emission spectra of MOFs. As shown in Fig. S9, the greatest spectral overlap occurs between PA and MOFs, and some extent overlaps exist in 4-NP/MOFs and 2,4-DNP/MOFs, whereas negligible or completely no spectral overlaps are observed for other NACs and MOFs. These results are consistent with the quenching efficiency of respective NACs for **1'** and **2'** in general.

To study the recyclability and stability of **1'** and **2'**, the quenching and recovery experiments of PA have been carried out. The used samples can be regenerated and reused via simple centrifugation and wash three times with ethanol. For these two compounds, the initial luminescent intensities and the quenching ability change slightly in 1−5 cycles (Fig. 8), the PXRD patterns confirmed their frameworks are retained after 5 cycles (Fig. S3).
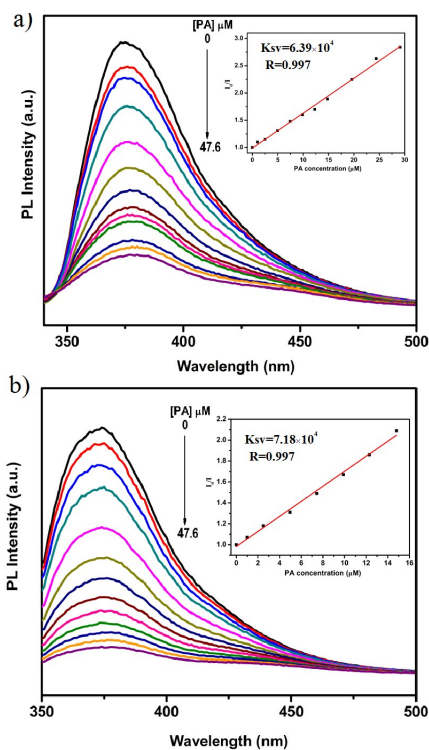
Fig. 7 a), b) Luminescent quenching of **1'** and **2'** dispersed in ethanol with gradual addition of 1 mM PA-ethanol solution, respectively (insert: Stern-Volmer plots at low PA concentrations).
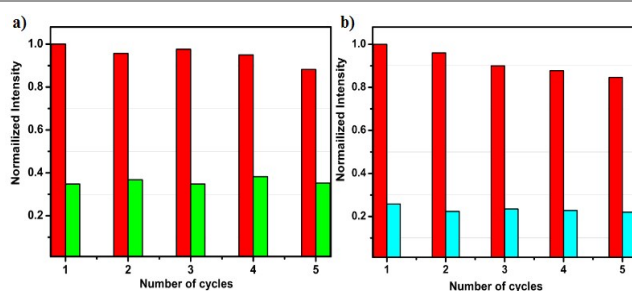
Fig. 8 The quenching and recovery test of micrometer-sized **1'** and **2'** dispersed in ethanol in the presence of PA solution (The red bars represent the initial fluorescence intensities, the green and the cyan bars represent the intensities upon the addition of PA (29.1 μM) for **1'** and **2'**, respectively).

Conclusions

In conclusion, two luminescent Zn-MOFs based on the rigid unsymmetrical tricarboxylate ligand H$_3$TPT have been prepared by modulating the solvent media. The discrepancies of coordination modes of zinc ions and TPT^{3-} ligands result in their distinct 3D frameworks, i.e. 4,8-connected alb-4,8-*C*2/*c* topology for **1** and 3,6-connected scu-3,6-*Pbcn* topology for **2**. These two MOFs exhibit high efficiency, recyclability and structural stability for the detection of NACs. Particularly, they have the potentialities for selective detection of hydroxy-substituted NACs including 4-NP, 2,4-DNP and PA over their methyl-substituted analogues. The fluorescence quenching response to NACs should be attributed to the resonance energy transfer process.

Acknowledgements

Notes and references

State Key Lab of Inorganic Synthesis and Preparative Chemistry, Jilin University, Changchun, 130012, P. R. China, E-mail: lijiyang@jlu.edu.cn; liangzq@jlu.edu.cn.
†Electronic Supplementary Information (ESI) available: X-ray crystallographic data for **1** and **2** in CIF format. The crystal data and structure refinement, and the selected bond lengths and angles for **1** and **2**. PXRD patterns, TGA, SEM and IR spectra. The asymmetric unit of 1 and **2**. The space filling structure of **2**. Fluorescent titrations of different volume of NACs in **1'** and **2'** suspensions. CCDC numbers are 1063673 and 1063674 for **1** and **2**, respectively. See DOI: 10.1039/b000000x/.

1. M. P. Suh, H. J. Park, T. K. Prasad and D.-W. Lim, *Chem. Rev.,* 2012, **112**, 782.
2. L. Schlapbach and A. Züttel, *Nature.,* 2001, **414**, 353.
3. H. Furukawa, N. Ko, Y. B. Go, N. Aratani, S. B. Choi, E. Choi, A. Ö. Yazaydin, R. Q. Snurr, M. O'Keeffe, J. Kim and O. M. Yaghi, *Science.,* 2010, **329**, 424.
4. J. R. Li, J. Sculley and H. C. Zhou, *Chem. Rev.,* 2012, **112**, 869.
5. B. L. Chen, S. C. Xiang and G. D. Qian, *Acc Chem. Res.,* 2010, **43**, 1115.
6. O. S. Wenger, *Chem. Rev.,* 2013, **113**, 3686.
7. Z. Z. Lu, R. Zhang, Y. Z. Li, Z. J. Guo and H. G. Zheng, *J. Am. Chem. Soc.,* 2011, **133**, 4172.
8. D. W. Feng, Z. Y. Gu, J. R. Li, H. L. Jiang, Z. W. Wei and H. C. Zhou, *Angew. Chem. Int. Ed.,* 2012, **51**, 10307.
9. A. Corma, H. García and F. X. Llabrés i Xamena, *Chem. Rev.,* 2010, **110**, 4606.
10. J. W. Liu, L. F. Chen, H. Cui, J. Y. Zhang, L. Zhang and C. Y. Su, *Chem. Soc. Rev.,* 2014, **43**, 6011.
11. Y. J. Cui, Y. F. Yue, G. D. Qian and B. L. Chen, *Chem. Rev.,* 2012, **112**, 1126.
12. J. Rocha, L. D. Carlos, F. A. Almeida Paz and D. Ananias, *Chem. Soc. Rev.,* 2011, **40**, 926.
13. E. Coronado and G. M. Espallargas, *Chem. Soc. Rev.,* 2013, **42**, 1525.
14. M. Kurmoo, *Chem. Soc. Rev.,* 2013, **42,** 1353.
15. P. X. Yin, J. Zhang, Y. Y. Qin, J. K. Cheng, Z. J. Li and Y. G. Yao, *CrystEngComm.* 2011, **13**, 3536.
16. Y. B. Go, X. Q. Wang, E. V. Anokhina and A. J. Jacobson, *Inorg. Chem.,* 2005, **44**, 8265.
17. Y. B. Dong, Y. Y. Jiang, J. Li, J. P. Ma, F. L. Liu, B. Tang, R. Q. Huang and S. R. Batten, *J. Am. Chem. Soc.,* 2007, **129**, 4520.
18. L. F. Ma, L. Y. Wang, D. H. Lu, S. R. Batten and J. G. Wang, *Cryst. Growth Des.,* 2009, **9**, 1741.
19. F. Y. Cui, K. L. Huang, Y. Q. Xu, Z. G. Han, X. Liu, Y. N. Chi and C. W. Hu, *CrystEngComm.,* 2009, **11**, 2757.
20. J. S. Qin, D. Y. Du, S. L. Li, Y. Q. Lan, K. Z. Shao and Z. M. Su, *CrystEngComm.,* 2011, **13**, 779.
21. X. R. Hao, X. L. Wang, K. Z. Shao, G. S. Yang, Z. M. Su and G. Yuan, *CrystEngComm.,* 2012, **14**, 5596.
22. M. Guo and Z. M. Sun, *J. Mater. Chem.,* 2012, **22**, 15939.
23. S. C. Chen, Z. H. Zhang, K. L. Huang, Q. Chen, M. Y. He, A. J. Cui, C. Li, Q. Liu and M. Du, *Cryst. Growth Des.,* 2008, **8**, 3437.
24. G. S. Yang, Z. L. Lang, H. Y. Zang, Y. Q. Lan, W. W. He, X. L. Zhao, L. K. Yan, X. L. Wang and Z. M. Su, *Comm. Commun.,* 2013, **49,** 1088.
25. C. P. Li and M. Du, *Chem.Comm.,* 2011, **47**, 5958.
26. A. Karmakar, G. M. D. M. Rúbio, M. F. C. Guedes da Silva, S. Hazra and A. J. L. Pombeiro, *Cryst. Growth Des.,* 2015. **15**, 4185.
27. J. G. Duan, M. Higuchi, C. C. Zou, W. Q. Jin and S. Kitagawa, *CrystEngComm.,* 2015, **17**, 5609.
28. M. D. Allendorf, C. A. Bauer, R. K. Bhakta and R. J. T. Houk, *Chem. Soc. Rev.,* 2009, **38**, 1330.
29. P. Y. Wu, J. Wang, C. He, X. L. Zhang, Y. T. Wang, T. Liu and C. Y. Duan, *Adv. Func. Mater.,* 2012, **22**, 1698.
30. B. L. Chen, Y. Yang, F. Zapata, G. N. Lin, G. D. Qian and E. B. Lobkovsky, *Adv. Mater.,* 2007, **19**, 1693.
31. Z. C. Hu, B. J. Deibert and J. Li, *Chem. Soc. Rev.,* 2014, **43**, 5815.
32. D. Banerjee, Z. C. Hu and J. Li, *Dalton. Trans.,* 2014, **43**, 10668.
33. A. J. Lan, K. H. Li, H. H. Wu, D. H. Olson, T. J. Emge, M. Ki, M. C. Hong and J. Li, *Angew. Chem., Int. Ed.,* 2009, **48**, 2334.
34. Y. S. Xue, Y. B. He, L. Zhou, F. J. Chen, Y. Xu, H. B. Du, X. Z. You and B. L. Chen, *J. Mater. Chem. A.* 2013, **1**, 4525.
35. C. Q. Zhang, L. B. Sun, Y. Yan, J. Y. Li, X. W. Song, Y. L. Liu and Z. Q. Liang, *Dalton. Trans.,* 2015, **44**, 230.
36. C. Q. Zhang, Y. Yan, Q. H. Pan, L. Sun, H. M. He, Y. L. Liu, Z. Q. Liang and J. Y. Li, *Dalton. Trans.,* 2015, **44**, 13340.
37. E. V. Alexandrov, V. A. Blatov, A. V. Kochetkov and D. M. Proserpio, *CrystEngComm.,* 2011, **13**, 3947.
38. V. A. Blatov, *Struct. Chem.,* 2012, **23**, 955.
39. E. C. P. Bruker AXS Inc., Madison, WI 53711-5373, USA, 2000.
40. G. M. Sheldrick, *Acta Crystallogr., Sect. A.,* 2008, **64**, 112.
41. C. A. Williams, A. J. Blake, C. Wilson, P. Hubberstey and M. Schröder, *Cryst. Growth Des.,* 2008, **8**, 911.
42. D. P. Yan, R. Gao, M. Wei, S. D. Li, J. Lu, D. G. Evans and X. Duan, *J. Mater. Chem. C.,* 2013, **1**, 997.
43. N. Zhao, F. X. Sun, H. M. He, J. T. Jia and G. S. Zhu, *Cryst. Growth Des.,* 2014, **14**, 1738.
44. S. S. Nagarkar, B. Joarder, A. K. Chaudhari, S. Mukherjee and S. K. Ghosh, *Angew. Chem., Int. Ed.,* 2013, **52**, 2881.
45. X. Z. Song, S. Y. Song, S. N. Zhao, Z. M. Hao, M. Zhu, X. Meng, L. L. Wu and H. J. Zhang, *Adv. Func. Mater.,* 2014, **24**, 4034.
46. S. Mukherjee, A. V. Desai, B. Manna, A. I. Inamdar and S. K. Ghosh, *Cryst. Growth Des.,* 2015. **15**, 4627.
47. B. Gole, A. K. Bar and P. S. Mukherjee, *Chem.-Eur. J.,* 2014, **20**, 2276.
48. S. S. Nagarkar, A. V. Desai and S. K. Ghosh, *Chem. Commun.,* 2014, **50**, 8915.

Two three-dimensional metal-organic frameworks **1** and **2** based on p-terphenyl-3,4",5-tricarboxylate acid (H_3TPT) were synthesized by controlling the solvent media. They show different structures in different solvents. These two MOFs exhibit ligand-based photoluminescence and high efficiency for the recyclable detection of nitroaromatic compounds (NACs).